Nat. Hazards Earth Syst. Sci. Discuss., doi:10.5194/nhess-2017-111, 2017
Manuscript under review for journal Nat. Hazards Earth Syst. Sci.
Discussion started: 3 April 2017

Natural Hazards and Earth System Sciences
Discussions

Criteria for the optimal selection of remote sensing images to map event landslides

Federica Fiorucci[1], Daniele Giordan[2], Michele Santangelo[1], Furio Dutto[3], Mauro Rossi[1], Fausto Guzzetti[1].

[1]Istituto di Ricerca per la Protezione Idrogeologica, Consiglio Nazionale delle Ricerche, via della Madonna Alta 126, 06128 Perugia, Italy
[2]Istituto di Ricerca per la Protezione Idrogeologica, Consiglio Nazionale delle Ricerche, Strada delle Cacce 73, 10135 Torino, Italy
[3]Servizio Protezione Civile della Città Metropolitana di Torino, Via Alberto Sordi 13, 10095 Grugliasco, Italy

Correspondence to: Federica Fiorucci (federica.fiorucci@irpi.cnr.it)

Abstract. We executed an experiment to determine the effects of image characteristics on event landslide mapping. In the experiment, we compared eight maps of the same landslide, the Assignano landslide, in Umbria, central Italy. Six maps were obtained through the expert visual interpretation of monoscopic and pseudo-stereoscopic (2.5D), ultra-resolution (3 × 3 cm) images taken on 14 April 2014 by a Canon EOS M photographic camera flown by an CarbonCore 950 hexacopter over the landslide, and of monoscopic and stereoscopic, true-colour and false-colour-composite, 1.84 × 1.84 m resolution images taken by the WorldView-2 satellite also on 14 April 2014. The seventh map was prepared through a reconnaissance field survey aided by a pre-event satellite image taken on 8 July 2013, available on Goggle Earth™, and by colour photographs taken in the field with a hand-held camera. The images were interpreted visually by an expert geomorphologist using the StereoMirror™ hardware technology combined with the ERDAS IMAGINE® and Leica Photogrammetry Suite (LPS) software. The eighth map, which we considered our reference showing the "ground truth", was obtained through a Real Time Kinematic differential GPS survey conducted by walking a GPS receiver along the landslide perimeter to capture geographic coordinates every about 5 m, with centimetre accuracy. The eight maps of the Assignano landslide were stored in a GIS, and compared adopting a pairwise approach. Results of the comparisons, quantified by the error index *E*, revealed that where the landslide signature was primarily photographical (in the landslide source and transport area) the best mapping results were obtained using the higher resolution images, and where the landslide signature was mainly morphometric (in the landslide deposit) the best results were obtained using the stereoscopic images. The ultra-resolution image proved very effective to map the landslide, with results comparable to those obtained using the stereoscopic satellite image. Conversely, the field-based reconnaissance mapping provided the poorest results, measured by large mapping errors, and confirmed the difficulty in preparing accurate landslide maps in the field. Albeit conducted on a single landslide, we maintain that our results are general, and provide useful information to decide on the optimal imagery for the production of event, seasonal and multi-temporal landslide inventory maps.

Nat. Hazards Earth Syst. Sci. Discuss., doi:10.5194/nhess-2017-111, 2017
Manuscript under review for journal Nat. Hazards Earth Syst. Sci.
Discussion started: 3 April 2017

Natural Hazards and Earth System Sciences Discussions

1 Introduction

Accurate detection of single landslides has different scopes, including landslide mapping (Di Maio and Vassallo, 2011; Manconi et al., 2014; Plank et al., 2016), landslide hazard analysis and risk assessment (Allasia et al., 2013), to support the installation of landslide monitoring systems (Tarchi et al., 2003; Teza et al., 2007; Monserrat and Crosetto, 2008; Giordan et al., 2013), and for landslide geotechnical characterization and modelling (Gokceoglu, 2005; Rosi et al., 2013). Mapping of single landslides can be executed using the same techniques and tools commonly used by geomorphologists to prepare landslide inventory maps i.e., thought field surveys (Santangelo et al., 2010) or the visual interpretation of monoscopic or stereoscopic aerial or satellite images (Brardinoni et al., 2003; Fiorucci et al., 2011; Ardizzone et al., 2013), of LiDAR-derived images (Ardizzone et al., 2007; Van Den Eeckhaut et al., 2007; Haneberg et al., 2009; Giordan et al., 2013; Razak et al., 2013; Niculita et al., 2016), or of ultra-resolution images acquired by Unmanned Aerial Vehicles (UAV, Giordan et al., 2015a, 2015b; Torrero et al., 2015). All these mapping techniques have inherent advantages and intrinsic limitations, which depend on the size and type of the landslides, and on the characteristics of the images, including their spatial and spectral resolutions (Fiorucci et al., 2011). As a result, landslide maps prepared exploiting one or more of the mentioned techniques are inevitably incomplete, and contain errors in terms of the position, size, and shape of the mapped landslides (Guzzetti et al., 2000; Galli et al., 2008, Santangelo et al., 2015).

Attempts have been made to evaluate the errors associated to different types of landslide inventory maps (Carrara et al., 1992; Ardizzone et al., 2002, 2007; Van Den Eeckhaut et al., 2007; Fiorucci et al., 2011; Santangelo et al., 2010; Mondini et al., 2013). Most of these attempts compare landslide maps prepared using aerial or satellite images to maps obtained through reconnaissance field mapping (Ardizzone et al., 2007; Fiorucci et al., 2011) or GPS surveys (Santangelo et al., 2010). Conversely, only a few authors have attempted to evaluate the influence of different types of imagery on landslide detection and mapping (Carrara et al., 1992).

In this work, we evaluate how images of different type and characteristics influence event landslide mapping. We do this by comparing eight maps of a single, rainfall-induced landslide near the village of Assignano, Umbria, central Italy. Seven maps of the same landslide were obtained using different techniques and images, including (i) a reconnaissance field survey, (ii) the interpretation of ultra-resolution images taken by an optical camera on-board an UAV, and (iii) the visual interpretation of VHR, monoscopic and stereoscopic, multispectral images taken by the WordView-2 satellite. These maps were compared to an eighth map considered to be the benchmark showing the “ground truth” i.e., the “true” position, shape and extent of the Assignano landslide. Based on the results of the map comparison, we infer the ability of different images, characterized by different spectral and spatial characteristics, to portray the landslide features that can be exploited for the visual detection and mapping of landslides.

Nat. Hazards Earth Syst. Sci. Discuss., doi:10.5194/nhess-2017-111, 2017
Manuscript under review for journal Nat. Hazards Earth Syst. Sci.
Discussion started: 3 April 2017

Natural Hazards and Earth System Sciences
Discussions

2 The Assignano landslide

For our study, we selected the Assignano landslide that was triggered by intense rainfall in December 2013 in the northwest-facing slope of the Assignano village, Umbria, central Italy (**Fig. 1**). The landslide is about 340 m long, 40 m wide in the transportation area, and 60 m wide in the deposition area, and is characterized by three distinct source areas, two located on the SW side of the landslide and third located on the NE side of the landslide. The source and transportation area has an overall length of about 230 m, and a width increasing from 10 to 40 m from the top of the source area to the bottom of the transportation area. Elevation in the landslide ranges from 276 m along the landslide crown, to 206 m at the lowest tip of the deposit. The source and transportation area is bounded locally by sub-vertical, 2 to 4-m high escarpments. In the landslide, terrain slope averages 11°, and is steeper (12°) in the source and transportation area than in the deposition area (9°). The landslide signature (Pike, 1988) is different in the different parts of the landslide. In the source and transport area the signature is predominantly photographical (radiometric), whereas in the landslide deposit it is mainly morphometric (topographic).

3 Image acquisition

On 14 April 2014, we conducted an aerial survey of the Assignano landslide using a "X" shaped frame octocopter with eight motors mounted on four arms (four sets of CW and CCW props) with a payload capacity of around one kilogram, and a flight autonomy of about 20 minutes. The UAV was equipped with a remotely controlled gimbal hosting a ©GoPro Hero 3 video camera and a Canon EOS M camera. We controlled the flight of the UAV manually, relaying on the real-time video stream provided by the ©GoPro. We kept the operational flight altitude of the UAV in the range between 70 and 100 m above the ground. This allowed the Canon EOS M camera to capture 97 digital colour images of the landslide area with a ground resolution of about 2-4 cm, with the single images having an overlap of about 70% and a side-lap of about 40%. For the accurate geocoding of the images, we positioned 13 red-and-white, four-quadrants square targets, 20 cm × 20 cm in size, outside and inside the landslide. We obtained the geographical location (latitude, longitude, elevation) of the 13 target centres using a Real Time Kinematic (RTK) Differential Global Positioning System (DGPS), with a horizontal error of less than 3 cm. We processed the 97 images using commercial, structure-from-motion software to obtain (i) a 3D point cloud, (ii) a Digital Surface Model (DSM), and (iii) a digital, monoscopic, ultra-resolution (ground sampling distance is 3 × 3 cm) ortho-rectified image in the visible spectral range, which we used for the visual mapping of the Assignano landslide (**Table 1**).

To map the landslide, we also used a stereoscopic pair of very-high resolution (VHR) images taken on 14 April 2014 i.e., the same day of the UAV survey, by the WorldView-2 satellite that operates at an altitude of 496 km, and collects 46-cm panchromatic, and 1.85-m eight-band, multispectral (coastal blue, blue, green, yellow, red, red edge, and near infrared-1,

Nat. Hazards Earth Syst. Sci. Discuss., doi:10.5194/nhess-2017-111, 2017
Manuscript under review for journal Nat. Hazards Earth Syst. Sci.
Discussion started: 3 April 2017

Natural Hazards and Earth System Sciences Discussions

near-infrared-2) imagery at 11-bit dynamic range, in the spectral range 0.400 – 1.040 µm. For the satellite, the rational polynomial coefficients (RPCs) are available, allowing for accurate photogrammetric processing of the images. We used the RPCs to generate 3D models of the terrain from the stereoscopic image pair. Exploiting the characteristics of the satellite image, we prepared four separate images for landslide mapping, namely, (i) a monoscopic, "true colour" (TC) image, (ii) a monoscopic false-colour-composite (FCC) image obtained from the composite near infrared, red and green (432), (iii) a TC stereoscopic pair, and (iv) a FCC stereoscopic pair. We prepared separate maps of the Assignano landslide through the visual interpretation of the four images (**Table 1**).

To compare the images obtained by the UAV and the WorldView-2 satellite, we co-registered the images, and we evaluated the co-registration on seven control points, obtaining a Distance Root Mean Square error, DRMS = 0.53 m, and a Circular Error Probability, $CEP_{50\%}$ = 0.42 m, which we consider adequate for landslide mapping, and for the map comparison.

4 Landslide mapping

We prepared eight maps of the Assignano landslide using different approaches, images and datasets, including two maps prepared through field surveys, four maps prepared through the visual interpretation of monoscopic and stereoscopic satellite images, and two maps prepared through the visual interpretation of the images taken during the UAV survey (**Table 1**).

The field mapping and the image interpretation were carried out by independent geomorphologists. The two geomorphologists who carried out the field activities i.e., the reconnaissance field mapping and the RTK-DGPS survey, were not involved in the visual interpretation of the satellite and the UAV images. Equally, the geomorphologist who interpreted visually the satellite and the UAV images did not take part in the field activities. Visual interpretation of the remotely-sensed images was performed by a single geomorphologist to avoid problems related to different interpretation skills by different interpreters (Carrara et al., 1992). We then compared the eight resulting maps of the Assignano landslide adopting a pairwise approach to quantify and evaluate the mapping differences.

The geomorphologist who interpreted visually the images was shown first the 1.84-m resolution, monoscopic satellite image, next the 1.84-m resolution stereoscopic satellite pair, and lastly the 3-cm resolution UAV images. The monoscopic and the stereoscopic satellite images were first shown in TC and then in FCC. Lastly, the interpreter was shown the draped ultra-resolution UAV image. Selection of the sequence of the images given to the geomorphologist for the expert driven visual interpretation was based on the assumption that for landslide mapping (i) the ultra-resolution monoscopic images provide more information than the 2-m monoscopic or stereoscopic images, (ii) for equal spatial resolution images, stereoscopic images provide more information than monoscopic images, and (iii) for equal image type (monoscopic, stereoscopic), the FCC images provide more information than the TC images. To prevent biases related to a possible previous knowledge of the landslide, the interpreter was not shown the results of the reconnaissance field mapping.

Nat. Hazards Earth Syst. Sci. Discuss., doi:10.5194/nhess-2017-111, 2017
Manuscript under review for journal Nat. Hazards Earth Syst. Sci.
Discussion started: 3 April 2017

Natural Hazards and Earth System Sciences Discussions

4.1 Field mapping

Field mapping of the Assignano landslide consisted in two synergic activities, (i) a reconnaissance field survey, and (ii) a RTK DGPS aided survey. First, the reconnaissance field survey was conducted by two geomorphologists (FF and MR) who observed the landslide and took photographs of the slope failure from multiple viewpoints, close to and far from the landslide. The geomorphologists draw a preliminary map of the landslide in the field exploiting the most recent satellite image available at the time in Google Earth™, which was taken on 8 July 2013 i.e., before the landslide. The reconnaissance filed mapping was then refined in the laboratory using the ground photographs taken in the field. We refer to this reconnaissance representation of the Assignano landslide as "Map B".

Next, the same two geomorphologists (FF and MR) conducted an RTK DGPS aided survey walking a Leica Geosystems GPS 1200 receiver along the landslide boundary, capturing 3D geographic coordinates every about 5 m, in 3D distance. For the purpose, we used the SmartNet ItalPoS real-time network service to transmit the correction signal from the GPS base station to the GPS roving station. The estimated accuracy obtained for each survey point measured along the landslide boundary was 2 to 5 cm, measured by the root mean square error (RMS), on the ETRF-2000 reference system. We refer to the cartographic representation of the Assignano landslide produced by the RTK DGPS survey as "Map A". We consider this map as the "ground truth", and we use it as a benchmark against which to compare the other maps. We acknowledge that mapping a landslide by walking a GPS receiver around its boundary is an error prone operation e.g., because in places the landslide boundary is not sharp, or clearly visible from the ground (Santangelo et al., 2010). However, we maintain this is the most reasonable working assumption, and that the geometrical information obtained by walking a GPS receiver along the landslide boundary was superior to the information obtained through the reconnaissance field mapping (Map B) (Santangelo et al., 2010).

4.2 Mapping through image interpretation

A trained geomorphologist (MS) used the three monoscopic images (i.e., the TC and FCC monoscopic satellite images, and the monoscopic ultra-resolution UAV image) to perform a heuristic, visual mapping of the Assignano landslide. For the purpose, the interpreter considered the photographic (colour, tone, mottling, texture) and geometrical (shape, size, pattern of individual terrain features, or sets of features) characteristics of the images (Antonini et al., 1999). In this way, the geomorphologist prepared (i) "Map C" interpreting visually the monoscopic, TC satellite image, (ii) "Map D" interpreting visually the monoscopic, FFC satellite image, and (iii) "Map G" interpreting visually the monoscopic, TC UAV image (**Table 1**).

Next, the interpreter used the two stereoscopic satellite images (i.e., the TC and FCC images) to prepare "Map E" and "Map F" (**Table 1**). In the stereoscopic images, the photographic and morphological information is combined, favouring the recognition of the landslide features through the joint analysis of photographic (colour, tone, mottling, texture), geometrical (shape, size, pattern of features), and morphological terrain features (curvature, convexity, concavity). To analyse visually

the stereoscopic satellite images, the interpreter used the StereoMirror™ hardware technology, combined with the ERDAS IMAGINE® and Leica Photogrammetry Suite (LPS) software. To map the landslide features in real-world, 3D geographical coordinates, the interpreter used a 3D floating cursor (Fiorucci et al., 2015).

To interpret the ultra-resolution UAV image, the interpreter overlaid ("draped") the image on Google Earth™. For the purpose, we first treated the UAV image with gdal2tiles.py software to obtain a set of image tiles compatible with the Google Earth™ terrain visualization platform, and we used the platform standard editing tools to digitize the landslide features. We refer to the representation of the Assignano landslide obtained through the visual interpretation of the ultra-resolution UAV image as "Map H".

For the visual interpretation of the satellite and the UAV images, the interpreter adopted a visualization scale in the range from 1:1000 to 1:6000, depending on the image spatial resolution (**Table 1**).

5 Results

Using the described mapping methods, and the available satellite and UAV images (**Table 1**), we prepared eight separate and independent cartographic representations of the Assignano landslide, shown in **Fig. 2** as Map A to Map H.

Considering the entire landslide, visual inspection of **Fig. 2** reveals that the maps most similar to the benchmark (Map A) are Map E, prepared examining the true colour (TC) stereoscopic satellite image, and Map F, prepared examining the false colour composite (FCC) stereoscopic satellite image. Conversely, the largest differences were observed for the landslide maps obtained through the reconnaissance field survey (Map B), and the visual interpretation of the monoscopic satellite images (Map C and Map D). Considering only the source and transportation areas (dark colours in **Fig. 2**), interpretation of the UAV ultra-resolution images resulted in the landslide maps most similar (Map G and Map H) to the benchmark (Map A). It is worth noticing the systematic lack in the mapping of one of the two secondary landslide source areas located in the SW side of the landslide, which was recognized only from the visual inspection of the ultra-resolution images taken by the UAV flight. In the field, this source area was characterized by small cracks along the escarpment and a limited disruption of the meadow, making it particularly difficult to detect and map. We argue that only the ultra-resolution images allowed for the detection of the cracks. Considering only the landslide deposit (light colours in **Fig. 2**), the landslide mapping that was more similar to the benchmark (Map A) was obtained interpreting the TC, stereoscopic satellite images (Map E). We also note that in most of the maps the landslide deposit was mapped larger (Map G, Map H) or much larger (Map B, Map C and Map D) than the benchmark (Map A).

Table 2 lists geometric measures of the mapped landslides, including the length, width, and area (i) of the entire landslide, (ii) of the landslide source and transportation area (dark colours in **Fig. 2**), and (iii) of the landslide deposit (light colours in **Fig. 2**). The length and width measurements were obtained in a GIS as the length and the width of the minimum oriented rectangle encompassing (i) the entire landslide, (ii) the landslide source and transportation area, and (iii) the landslide deposit. Our benchmark (Map A) has a total area $A_L = 1.1 \times 10^4$ m^2, and is $L_{LS} = 362$ m long and $W_{LS} = 71$ m wide. Amongst

Nat. Hazards Earth Syst. Sci. Discuss., doi:10.5194/nhess-2017-111, 2017
Manuscript under review for journal Nat. Hazards Earth Syst. Sci.
Discussion started: 3 April 2017

Natural Hazards and Earth System Sciences Discussions

the other seven maps (Map B to Map H in **Fig. 2**), the largest landslide is shown in Map B, obtained through the reconnaissance field mapping, and has $A_L = 1.91\times10^4$ m^2, 71.1% larger than the benchmark. Conversely, the smallest landslide is shown in Map F, with $A_L = 1.1\times10^4$ m^2, 4.6% smaller than the benchmark. The longest and largest landslide is found in Map C, with $L_{LS} = 405$ m (11% longer than the benchmark) and $W_{LS} = 113$ m (60% wider than the benchmark).

Considering the source and transportation area, in Map A (the benchmark) $A_{LS} = 5.4\times10^3$ m^2, $L_{LS} = 228$ m, and $W_{LS} = 52$ m. The largest representation of the source and transportation area is found in Map B (reconnaissance field mapping) with $A_{LS} = 7.4\times10^3$ m^2, 36.9% larger than the benchmark, and the smallest source and transportation area is found in Map G, with $A_{LS} = 5.2\times10^3$ m^2, 3.6% smaller than the benchmark. The longest source and transportation area is found in Map F, with $L_{LS} = 239$ m, 5% longer than the benchmark, and the shortest source and transportation area is shown in Map C, with $L_{LS} = 206$ m, 9.7% shorter than the benchmark. The largest source and transportation area is shown in Map B, $W_{LS} = 60$ m, 15.7% wider than Map A, and the narrowest source and transportation area is in Map C, $L_{LS} = 44$ m, 15.3% narrower than the benchmark. Considering instead only the landslide deposit, our benchmark (Map A) has $A_{LD} = 5.7\times10^3$ m^2, $L_{LS} = 153$ m, and $W_{LS} = 61$ m. The largest deposit is shown in Map B (reconnaissance field mapping) and has $A_{LD} = 1.2\times10^4$ m^2, 103.4% larger than the benchmark, whereas the smallest landslide deposit is shown in Map F, with $A_{LD} = 4.6\times10^3$ m^2, 19.8% smaller than the benchmark. Analysis of the length and width of the landslide deposit reveals that Map C shows the longest deposit, $L_{LS} = 206$ m, 35% longer than the benchmark, and Map H shows the shortest deposit, $L_{LS} = 122$ m, 20.2% shorter than the benchmark. Similarly, the largest landslide deposit is shown in Map C, $W_{LS} = 112$ m, 82.8% wider than the benchmark, and the narrowest landslide deposit is portrayed in Map E, $W_{LS} = 56$ m, 8.2% less than the benchmark.

To compare quantitatively the different landslide maps, we use the error index *E* proposed by Carrara et al. (1992), adopting the pairwise comparison approach proposed by Santangelo et al. (2015). The index provides an estimate of the discrepancy (or similarity) between corresponding polygons in two maps, and is defined as:

$$E = \frac{(A \cup B) - (A \cap B)}{(A \cup B)};\ 0 \le E \le 1, \quad (1)$$

where, A and B are the areas of two corresponding polygons in the compared maps, and ∪ and ∩ are the geographical (geometric) union and intersection of the two polygons, respectively. *E* spans the range from 0 (perfect matching) to 1 (complete mismatch).

We compared the eight maps of the Assignano landslide (**Fig. 2**) adopting a pairwise approach, and considering first only the landslide source and transportation area, next only the landslide deposit, and lastly the entire landslide. **Fig. 3** summarizes the 84 values of the error index *E*, 28 for the landslide source and transportation area (**Fig. 3 I**), 28 for the landslide deposit (**Fig. 3 II**), and 28 for the entire landslide (**Fig. 3 III**). On average, the source and transportation area exhibits values of the error index smaller than the values found in the landslide deposit. This indicates that in the source and transportation area the landslide maps are more similar than in the landslide deposit. Inspection of **Fig. 3 I**, reveals a decrease of the error index in the source and transportation area for the maps obtained interpreting the available images (from Map C to Map H), compared to our benchmark obtained through the RTK DGPS survey ($0.38 < E < 0.15$), with Map G obtained interpreting the TC,

monoscopic, ultra-resolution UAV image. In the landslide deposit (**Fig. 3 II**), the minimum difference ($E = 0.21$) was found comparing the benchmark to Map E, obtained through the interpretation of the stereoscopic TC satellite image, and the largest difference ($E = 0.52$) was found comparing the benchmark to Map C, prepared interpreting the TC, monoscopic, satellite image.

Comparison of the maps obtained through the interpretation of the monoscopic images (Map C and Map D), and the maps obtained through the interpretation of stereoscopic (Map E and Map F) or ultra-resolution images (Map G and Map H), reveals a generally poor agreement, which is slightly worse in the landslide deposit. In particular, $0.31 \leq E \leq 0.44$ in the source and transportation area (**Fig. 3I**), and $0.43 \leq E \leq 0.63$ in the landslide deposit (**Fig. 3II**). Map C and Map D are very similar, with a mapping error $E = 0.17$. Maps obtained through the interpretation of stereoscopic satellite images (Map E and Map F, prepared using TC and FCC images, respectively), and maps prepared by interpreting the UAV images (Map G and Map H), exhibit a generally good agreement. In particular, $0.14 \leq E \leq 0.26$ in the landslide source and transportation area, and $0.15 \leq E \leq 0.38$ in the landslide deposit. The reconnaissance field mapping (Map B) exhibited the largest differences compared to all the other maps ($0.63 \leq E \leq 0.45$) in the landslide source and transportation area, and $0.44 \leq E \leq 0.73$ in the landslide deposit. The large values of E in the landslide deposit is probably due to lack of visibility of part of the landslide toe in the field.

6 Discussion

We discuss the ability of the different images used to detect and map the Assignano landslide (**Fig. 1**) to resolve the landslide photographical and morphological signatures, considering separately the image spatial and spectral resolutions, and the image type i.e., monoscopic, stereoscopic, or pseudo-stereoscopic. We treat each of the three factors separately, keeping the other two factors constant. To evaluate the influence of the image spatial resolution on landslide mapping, we compare to our benchmark (Map A) two true-colour (TC) monoscopic maps (Map C and Map G), and two TC stereoscopic maps (Map E and Map H). Next, to evaluate the influence of the image spectral resolution on the landslide mapping, we compare to the benchmark (Map A) the TC and the false-colour-composite (FCC) monoscopic maps (Map C and Map D), and the corresponding TC and FCC stereoscopic maps (Map E and Map F). Lastly, to assess the influence of the type of image (i.e., monoscopic, stereoscopic, pseudo-stereoscopic) on the landslide mapping, we compare to the benchmark (Map A) the monoscopic (Map C) and the stereoscopic (Map E) TC maps (**Fig. 4A**), the two FCC maps (Map D and Map F) (**Fig. 4B**), and the maps obtained interpreting the ultra-resolution images captured by the UAV (Map G and Map H). **Fig. 3** summarizes the mapping errors E obtained by the pairwise comparisons of the eight landslide maps shown in **Fig. 2**.

We first evaluate the role of the image spatial resolution in the production of the different maps of the Assignano landslide. Inspection of **Fig. 3 I** reveals that the maps of the landslide source and transportation area obtained from images characterized by the highest spatial resolution (i.e., Map G and Map H) exhibits the smallest errors ($E \leq 0.16$), when compared to the benchmark (Map A). The mapping error obtained for Map C (TC, monoscopic, $E = 0.38$) is 2.5 times larger

Nat. Hazards Earth Syst. Sci. Discuss., doi:10.5194/nhess-2017-111, 2017
Manuscript under review for journal Nat. Hazards Earth Syst. Sci.
Discussion started: 3 April 2017

Natural Hazards and Earth System Sciences Discussions

than the error obtained using the ultra-resolution images taken by the UAV (Map G, $E = 0.15$, and Map H, $E = 0.16$), whereas the error obtained from Map E (TC, stereoscopic, $E = 0.23$) is smaller, and about 1.5 times larger than the error obtained for Map H (TC, pseudo-stereoscopic, $E = 0.16$). In the landslide deposit (**Fig. 3 II**), the map obtained exploiting the monoscopic, TC satellite image (Map C) exhibits an error $E = 0.52$, 1.7 times larger than the error obtained using Map G (TC, monoscopic UAV, $E = 0.30$). Conversely, the error is smaller in the map obtained from the 2-m spatial resolution, stereoscopic TC satellite image (Map E, $E = 0.21$) than from the 3-cm spatial resolution, pseudo-stereoscopic image taken by the UAV (Map H, $E = 0.30$). Collectively, the pairwise comparisons highlights a significant improvement of the quality of the mapping of the landslide features that exhibits a distinct photographical signature, most visible in the source and transportation area of the Assignano landslide, with an increase of the image spatial resolution (**Fig. 3**). Use of the ultra-resolution image captured by the UAV did not result in a significant improvement of the mapping in the deposition area of the Assignano landslide, where the landslide exhibits a distinct morphological signature. We further observe that most of the landslide parts that were not identified in the maps prepared using the satellite image are covered by vegetation, locally bounded by small and thin cracks with an average width smaller than the size of the 2×2 m pixel. In the satellite image, the cracks are located in pixels containing a mix of vegetation and bare soil, making it difficult for the interpreter to recognize the cracks.

Next, we evaluate the effectiveness of the image spectral resolution, and for the purpose we examine the mapping errors of Maps C and Map E (TC), and of Map D and Map F (FCC). The mapping of the source and transportation area prepared using the false-colour-composite (FCC) images (Map D and Map F) resulted in smaller errors than the mapping prepared using the corresponding true-colour (TC) images (Map C and Map E), for both monoscopic and stereoscopic images (**Fig. 3 I**). In the source and transportation area, the false-colour-composite emphasized the presence or absence of the vegetation, and contributed locally to highlight the typical photographical signature of the landslide, which helped the photo-interpreter to detect and map the slope failure. Conversely, in the landslide deposition area (**Fig. 3 II**) use of the FCC images did not result in a systematic reduction of the mapping error, when compared to the TC images. We conclude that use of additional information contributed by the Near Infrared (NIR) band did not improve the quality of the mapping.

Next, we evaluate the influence of the image type (i.e., monoscopic, stereoscopic, pseudo-stereoscopic) on the mapping error by comparing (i) the TC images (Map C and Map E), (ii) the FCC images (Map D and Map F), and (iii) the ultra-resolution UAV image (Map G and Map H). Comparison of the TC, monoscopic (Map C) and stereoscopic (Map E) images revealed a mapping error for the entire landslide $E = 0.48$, with the mismatch significantly larger in the deposition area ($E = 0.59$) than in the source and transpiration area ($E = 0.45$) (**Fig. 3**). A similar result was obtained comparing the FCC, monoscopic (Map D) and stereoscopic (Map F) images, with a mapping error for the entire landslide $E = 0.44$, and again the mismatch significantly larger in the deposition area ($E = 0.60$) than in the source and transpiration area ($E = 0.36$). In the deposition area, where the morphological signature of the Assignano landslide is strongest, the mapping error obtained comparing our benchmark (Map A) to the landslide maps prepared using the monoscopic images (Map C and Map D) is 2 times larger than the error observed for the maps prepared using the corresponding stereoscopic images (Map E and Map F). The differences

are smaller in the source and transportation area, where the morphological signature of the landslide is less distinct. Direct comparison of Map E (TC, stereoscopic) and Map F (FCC, stereoscopic) for the entire landslide reveals a very small mapping error ($E = 0.15$), indicating the similarity of the two maps, which were also very similar to the benchmark (Map A), $E \leq 0.20$.

Comparison for the entire landslide of the maps prepared using the ultra-resolution images captured by the UAV (Map G and Map H) exhibits the smallest error of all the pairwise comparisons ($E = 0.08$) (**Fig. 3 III**), indicating the large degree of matching between the two maps. The degree of matching is only marginally smaller in the source and transportation area, and in the deposition area ($E = 0.15$). When compared to our benchmark (Map A), Map G and Map H exhibit a small error ($E = 0.19$) for the entire landslide, which is larger in the deposition area ($E \leq 0.30$) and slightly smaller in the source and transport area ($E \leq 0.15$). Interestingly, the mismatch with Map A (the benchmark) is lower for the monoscopic (Map G) than for the pseudo-stereoscopic (Map H) map. The finding highlights the lack of an advantage in using a pseudo-stereoscopic (2.5D) image for mapping the Assignano landslide. We attribute this result to the low resolution of the (pre-event) DEM used to drape the ultra-resolution image for visualization purposes, which did not add any significant morphological information to the expert visual interpretation.

Joint analysis of **Fig. 2B** and **Fig. 3** reveals that, when compared to our benchmark (Map A), the reconnaissance field mapping (Map B) exhibited the largest mapping error of all the performed pairwise comparisons, with $E = 0.45$ in the source and transportation area, $E = 0.67$ in the landslide deposit, and $E = 0.55$ for the entire landslide. We note than an error of $E = 0.50$ indicates that 50% of the landslide area in one map (Map B, in this case) does not overlay with the other map (Map A, the benchmark, in this case). Our results are similar to the results of tests performed to compare field-based landslide maps against GPS-based surveys of single landslides (Santangelo et al., 2010), the visual interpretation of very-high resolution stereoscopic satellite images (Ardizzone et al., 2013), or the semi-automatic processing of monoscopic satellite images (Mondini et al., 2013), and confirm the inherent difficulty in preparing accurate landslide maps in the field, unless the mapping is supported by a GPS survey or a similar technology.

Our experiment showed that the mapping of the Assignano landslide obtained exploiting the ultra-resolution images captured by the UAV (Map G and Map H) was comparable to the maps obtained using the high resolution stereoscopic satellite image (Map E and Map F), and to the ground-based RTK DGPS survey (Map A, the benchmark). We conclude that ultra-resolution images captured by an UAV are well suited to map event landslides, at least in physiographical settings similar to the one of our study area, and for landslides similar to the Assignano landslide (**Fig. 1**).

For event landslide mapping, selection between ultra-resolution pseudo-stereoscopic UAV images and very-high resolution stereoscopic satellite images depends on (i) the extent of the investigated area, (ii) the available resources, including time and budget, and (iii) the accessibility to the study area. The selection is largely independent from the landslide signature, at least for landslides similar to the Assignano landslide. From an operational perspective, modern multi-rotor UAVs allow for the acquisition of ultra-resolution images over small areas in a limited time, and at very low costs. UAV-based surveys are flexible in their acquisition planning, and partly independent from the local lighting conditions, including the cloud cover. As

Nat. Hazards Earth Syst. Sci. Discuss., doi:10.5194/nhess-2017-111, 2017
Manuscript under review for journal Nat. Hazards Earth Syst. Sci.
Discussion started: 3 April 2017

Natural Hazards and Earth System Sciences Discussions

a drawback, UAVs are strongly (and negatively) affected by wind speed and weather conditions, they allow for a limited flight time (currently approximately 20 minutes in optimal conditions), which is reduced in bad weather conditions and in cold environments, and a have typically limited data storage capacity. Further, it must be possible for the pilot to be at the same time near to the area to be surveyed and to maintain a safe distance from the UAV, a condition that may be difficult to attain in remote or in mountain areas. Collectively, the intrinsic advantages and limitations of modern UAVs make the technology potentially well suited for the acquisition of ultra-resolution images for event, seasonal, and multi-temporal mapping of single landslides, of multiple landslides in a single slope, or in a relatively small area (a few hectares). Use of UAVs becomes impracticable with the increasing extent of the study area, largely due to (i) the operational difficulty of flaying UAVs over large areas, and (ii) the acquisition and image processing time and associated cost, which increase rapidly with the size of the study area (**Table 3**). On the other hand, very-high resolution, stereoscopic satellite images have also advantages and limitations for the production of event, seasonal and multi-temporal landslide inventory maps (Guzzetti et al., 2012). The main advantage of the satellite images is that they cover large or very areas (tens to hundreds of square kilometres) in a single frame with a sub-metric resolution well suited for landslide mapping through the expert visual interpretation of the images (Ardizzone et al., 2013). On the other hand, limitations remain due to distortions caused by different off-nadir angles in successive scenes, and to difficulties – in places severe – to obtaining suitable (e.g., cloud-free) images at the required time intervals. This is particularly problematic for the production of seasonal and multi-temporal landslide maps.

Information on the photographic or topographic signature of the typical, or most abundant, landslides in an area, is important to help select the optimal characteristics of the images best suited for the production of an event, seasonal or multi-temporal landslide inventory map. Use of images of non-optimal characteristics for a typical landslide signature in an area may condition the quality (i.e., completeness, geographic and thematic accuracy) of the landslide inventory. Where possible, we recommend that the acquisition of the images used for the production of event, seasonal or multi-temporal landslide inventory maps is planned considering the typical landslide signature, in addition to the scope of the mapping, and the size and complexity of the study area (**Table 3**).

7 Concluding remarks

We executed an experiment aimed at determining and measuring the effects of the image characteristics on event landslide mapping. In the experiment, we compared landslide maps obtained (i) through the expert visual interpretation of an ultra-resolution image taken by an UAV with a ground resolution of 3 × 3 cm, and monoscopic and stereoscopic true-colour and false-colour-composite (1.84 × 1.84 m) images taken by the WorldView-2 satellite, (ii) a reconnaissance field survey of the landslide, and (iii) an accurate survey of the landslide obtained by walking a GPS receiver along the landslide boundary. We conducted the experiment on a the Assignano landslide (**Fig. 1**) triggered by intense rainfall in December 2013 in the northwest-facing slope of the Assignano village, Umbria, central Italy. The landslide exhibited a predominant photographical

(radiometric) signature in the source and transport area, and a more distinct morphological (topographic) signature in the deposition area. The results of our mapping experiment allow for the following conclusions.

First, in the landslide source and transport area, where the signature of the slope failure was primarily photographical (radiometric), mapping errors (Carrara et al., 1992; Santangelo et al., 2015) decreased with the increase of the spatial resolution of the images used for the expert visual detection and mapping of the landslide. In the same area, the image photographic (radiometric) characteristics (true-colour, false-colour-composite) and the image type (monoscopic, stereoscopic) played a minor role in augmenting the quality of the landslide map. Conversely, in the deposition area, where the signature of the landslide was primarily morphological (topographical), mapping errors decreased using stereoscopic images that allowed detecting topographic features distinctive of the landslide. In the same area, a better spatial and spectral resolution did not contribute significantly to reducing the mapping errors.

Second, use of the stereoscopic satellite images resulted in more accurate landslide maps (lower error index *E*) than the corresponding monoscopic images in the landslide deposition area, where the signature of the landslide was primarily morphometric (topographic). This was expected, as the stereoscopic vision allowed to better capture the 3D terrain features typical of a landslide (Pike, 1988), including curvature, convexity and concavity. Conversely, visual examination of the false-colour-composite images resulted in more accurate maps than the corresponding true-colour images in the landslide source and transport area, where the signature of the landslide was primarily photographic (radiometric). This was also expected (Guzzetti et al., 2012). Expert visual interpretation of pseudo-stereoscopic ultra-resolution image failed to provide better results than the corresponding monoscopic ultra-resolution image, most probably because the DEM used to drape (overlay) the image on the terrain information was of low resolution.

Third, the ultra-resolution (3 × 3 cm) image captured by the photographic camera flown on-board the Unmanned Aerial Vehicle (UAV) proved very effective to detect and map the landslide. The expert visual interpretation of the monoscopic ultra-resolution image provided mapping results comparable to those obtained using the about 2-m resolution, stereoscopic satellite image.

Fourth, a comparative analysis of the technological constrains and the costs of acquisition and processing of ultra-resolution imagery taken by UAV and of high, or very-high resolution imagery taken by optical satellites revealed that the ultra-resolution images are well suited to map single event landslides, clusters of landslides in a single slope, or a few landslides in nearby slopes in a small area, and prove unsuited to cover large, and very large areas where the stereoscopic satellite images provide the most effective option.

Fifth, our field-based reconnaissance mapping (Map B) provided the least accurate mapping results, measured by the largest mapping error ($E = 0.55$ for the entire landslide) when compared to the benchmark map (**Fig. 3**). Our results confirm the inherent difficulty in preparing accurate landslide maps in the field through a reconnaissance mapping (Santangelo et al., 2010).

Although we conducted our study on a single landslide (**Fig. 1**), we maintain that the findings are general, and can be useful to decide on the optimal imagery and technique to be used when planning the production of a landslide inventory map. We

emphasize that the technique and imagery used to prepare landslide inventory maps should be selected depending on multiple factors, including (i) the typical or predominant landslide signature (photographic or morphological), (ii) the scale and size of the study area (a single slope, a small catchment, a large region), and (iii) the scope of the mapping (event, seasonal, multi-temporal, Guzzetti et al., 2012).

Author contributions. Federica Fiorucci and Daniele Giordan designed the experiment and defined the scientific objectives of the study. Federica Fiorucci performed the data analysis. Federica Fiorucci, Michele Santangelo and Fausto Guzzetti wrote the paper. Mauro Rossi, Federica Fiorucci, Furio Dutto and Danile Giordan carried out the field activities. All authors discussed the results and commented on the paper.

Competing interests. The authors declare that they have no conflict of interest.

Acknwoledgements. Federica Fiorucci and Michele Santangelo were supported by a grant of Italian Dipartimento della Protezione Civile. We thank Andrea Bernini and Mario Truffa, Servizio Protezione Civile della Città Metropolitana di Torino, for flying the UAV over the Assignano landslide.

References

Allasia, P., Manconi, A., Giordan, D., Baldo, M., and Lollino, G.: ADVICE: a new approach for near-real-time monitoring of surface displacements in landslide hazard scenarios. Sensors, 13, 7, 8285-8302, https://doi.org/10.3390/s130708285, 2013.

Allum, J. A. E.: Photogeology and regional mapping. Pergamon, 107 pp., 1966.

Antonini, G., Ardizzone, F., Cardinali, M., Galli, M., Guzzetti, F. and Reichenbach, P.: Surface deposits and landslide inventory map of the area affected by the 1997 Umbria-Marche earthquakes, Boll. Soc. Geol. It., 121, 843-853, 2002.

Ardizzone, F., Cardinali, M., Carrara, A., Guzzetti, F., and Reichenbach, P.: Impact of mapping errors on the reliability of landslide hazard maps, Nat. Hazards Earth Syst. Sci., 2, 3-14, https://doi.org/10.5194/nhess-2-3-2002, 2002.

Ardizzone, F., Cardinali, M., Galli, M., Guzzetti, F., and Reichenbach, P.: Identification and mapping of recent rainfall-induced landslides using elevation data collected by airborne Lidar, Nat. Hazards Earth Syst. Sci., 7, 637-650, https://doi.org/10.5194/nhess-7-637-2007, 2007.

Ardizzone, F., Fiorucci, F., Santangelo, M., Cardinali, M., Mondini, A.C., Rossi, M., Reichenbach, P., and Guzzetti, F.: Very-high resolution stereoscopic satellite images for landslide mapping. C. Margottini, P. Canuti, K. Sassa (Eds.), Landslide Science and Practice, Landslide Inventory and Susceptibility and Hazard Zoning, 1, Springer, Heidelberg, Berlin, New York, 95–101, https://doi.org/10.1007/978-3-642-31325-7_12, 2013.

Brardinoni, F., Slaymaker, O., and Hassan, M.A.: Landslides inventory in a rugged forested watershed: a comparison between air-photo and field survey data, Geomorphology, 54, 179-196, https://doi.org/10.1016/S0169-555X(02)00355-0, 2003.

Carrara, A., Cardinali, M., and Guzzetti, F.: Uncertainty in assessing landslide hazard and risk, ITC Journal, 2, 172-183, 1992.

Di Maio, C., and Vassallo, R.: Geotechnical characterization of a landslide in a Blue Clay slope, Landslides, 8, 17-32, https://doi.org/10.1007/s10346-010-0218-8, 2011.

Fiorucci, F., Cardinali, M., Carlà, R., Rossi, M., Mondini, A. C., Santurri, L., Ardizzone, F., and Guzzetti, F.: Seasonal landslides mapping and estimation of landslide mobilization rates using aerial and satellite images, Geomorphology, 129, 59-70, https://doi.org/10.1016/j.geomorph.2011.01.013, 2011.

Fiorucci, F.; Ardizzone, F.; Rossi, M.; Torri, D.: The Use of Stereoscopic Satellite Images to Map Rills and Ephemeral Gullies. Remote Sens., 7, 14151-14178, https://doi.org/10.3390/rs71014151, 2015.

Galli, M., Ardizzone, F., Cardinali, M., Guzzetti, F., and Reichenbach, P.: Comparing landslide inventory maps, Geomorphology, 94, 268–289, https://doi.org/10.1016/j.geomorph.2006.09.023, 2008.

Giordan, D., Allasia, P., Manconi, A., Baldo, M., Santangelo, M., Cardinali, M., Corazza, A., Albanese, V., Lollino, G., and Guzzetti, F.: Morphological and kinematic evolution of a large earthflow: The Montaguto landslide, southern Italy, Geomorphology, 187, 61-79, https://doi.org/10.1016/j.geomorph.2012.12.035, 2013.

Giordan, D., Manconi, A., Allasia, P., and Bertolo, D.: Brief Communication: On the rapid and efficient monitoring results dissemination in landslide emergency scenarios: the Mont de La Saxe case study, Nat. Hazards Earth Syst. Sci., 15, 2009-2017, https://doi.org/10.5194/nhess-15-2009-2015, 2015.

Giordan, D., Manconi, A., Facello, A., Baldo, M., dell'Anese, F., Allasia, P., and Dutto, F.: Brief Communication: The use of an unmanned aerial vehicle in a rockfall emergency scenario, Nat. Hazards Earth Syst. Sci., 15, 163-169, https://doi.org/10.5194/nhess-15-163-2015, 2015.

Gokceoglu, C., Sonmez, H., Nefeslioglu, H. A., Duman, T. Y., Can, T.: The 17 March 2005 Kuzulu landslide (Sivas, Turkey) and landslide-susceptibility Map of its near vicinity. Engineering Geology, 81, 1, 65-83, https://doi.org/10.1016/j.enggeo.2005.07.011, 2005.

Guzzetti, F., Ardizzone, F., Cardinali, M., Rossi, M., and Valigi, D.: Landslide volumes and landslide mobilization rates in Umbria, central Italy, Earth Planet. Sc. Lett., 279, 222-229, https://doi.org/10.1016/j.epsl.2009.01.005, 2009.

Guzzetti, F., Cardinali, M., Reichenbach, P., Cipolla, F., Sebastini, C., Galli, M., and Salvati, P.: Landslides triggered by the 23 November 2000 rainfall event in the Imperia Province, Western Liguria, Italy, Eng. Geol., 73, 229–245, https://doi.org/10.1016/j.enggeo.2004.01.006, 2000.

Guzzetti, F., Mondini, A. C., Cardinali, M., Fiorucci, F., Santangelo, M., and Chang, K.-T.: Landslide inventory maps: new tools for and old problem, Earth-Sci. Rev., 112, 42-66, https://doi.org/10.1016/j.earscirev.2012.02.001, 2012.

Haneberg, W. C., Cole, W. F., and Kasali, G.: High-resolution lidarbased landslide hazard mapping and modeling, UCSF Parnassus Campus; San Francisco, USA, B. Eng. Geol. Environ., 68, 263-276, https://doi.org/10.1007/s10064-009-0204-3, 2009.

Keaton, J. R. and DeGraff, J. V.: Surface observation and geologic mapping, in: Landslides: Investigation and Mitigation, Transportation Research Board, Washington, D.C., 178-230, 1996.

Manconi, A., Casu, F., Ardizzone, F., Bonano, M., Cardinali, M., De Luca, C., Gueguen, E., Marchesini, Parise, M., Vennari C., Lanari, R., Lanari, R.: Brief Communication: Rapid mapping of landslide events: the 3 December 2013 Montescaglioso landslide, Italy. Natural Hazards and Earth System Sciences, 14, 7, 1835, https://doi.org/10.5194/nhess-14-1835-2014, 2014.

Miller, C. V., Photogeology. Mac Graw Hill Book Company Inc., London, 1961.

Mondini, A. C., Marchesini, I., Rossi, M., Chang, K.-T., Pasquariello, G., and Guzzetti, F.: Bayesian framework for mapping and classifying shallow landslides exploiting remote sensing and topographic data, Geomorphology, 201, 135-147, https://doi.org/10.1016/j.geomorph.2013.06.015, 2013.

Niculiţă, M.: Automatic landslide length and width estimation based on the geometric processing of the bounding box and the geomorphometric analysis of DEMs, Nat. Hazards Earth Syst. Sci., 16, 2021-2030, https://doi.org/10.5194/nhess-16-2021-2016, 2016.

Notti, D., Davalillo, J. C., Herrera, G., and Mora, O.: Assessment of the performance of X-band satellite radar data for landslide mapping and monitoring: Upper Tena Valley case study, Nat. Hazards Earth Syst. Sci., 10, 1865-1875, https://doi.org/10.5194/nhess-10-1865-2010, 2010.

Pike, R.J.: The geometric signature: quantifying landslide-terrain types from digital elevation models, Mathematical Geology, 20, 5, 491-511, 1988.

Plank, S.: Rapid damage assessment by means of multi-temporal SAR—A comprehensive review and outlook to Sentinel-1, Remote Sensing, 6, 6, 4870-4906, https://doi.org/10.3390/rs6064870, 2014.

Ray, R. G.: Aerial Photographs in Geological Interpretation and Mapping. Geological Survey Professional Paper 373, Washington, USA, 1960.

Razak, K. A., Santangelo, M., Van Westen, C. J., Straatsma, M. W., and de Jong, S. M.: Generating an optimal DTM from airborne laser scanning data for landslide mapping in a tropical forest environment, Geomorphology, 190, 112-125, https://doi.org/10.1016/j.geomorph.2013.02.021, 2013.

Rosi, A., Vannocci, P., Tofani, V., Gigli, G., Casagli, N.: Landslide characterization using satellite interferometry (PSI), geotechnical investigations and numerical modelling: the case study of Ricasoli Village (Italy). Int. J. Geosci., 4, 904-918, https://doi.org/10.4236/ijg.2013.45085, 2013.

Santangelo, M., Cardinali, M., Rossi, M., Mondini, A. C., and Guzzetti, F.: Remote landslide mapping using a laser rangefinder binocular and GPS, Nat. Hazards Earth Syst. Sci., 10, 2539-2546, https://doi.org/10.5194/nhess-10-2539-2010, 2010.

Santangelo, M., Marchesini, I., Bucci, F., Cardinali, M., Fiorucci, F., and Guzzetti, F.: An approach to reduce mapping errors in the production of landslide inventory maps, Nat. Hazards Earth Syst. Sci., 15, 2111-2126, https://doi.org/10.5194/nhess-15-2111-2015, 2015.

Tarchi, D., Casagli, N., Fanti, R., Leva, D. D., Luzi, G., Pasuto, A., Pieraccini, M., Silvano, S.: Landslide monitoring by using ground-based SAR interferometry: an example of application to the Tessina landslide in Italy. Eng. Geol., 68, 1, 15-30, https://doi.org/10.1016/S0013-7952(02)00196-5, 2003.

Teza, G., Galgaro, A., Zaltron, N., Genevois, R.: Terrestrial laser scanner to detect landslide displacement fields: a new approach. Int. J. Remote Sensing, 28, 16, 3425-3446, https://doi.org/10.1080/01431160601024234, 2007.

Torrero, L. Seoli, L. Molino, A. Giordan, D. Manconi, A. Allasia, P. and Baldo, M. The Use of Micro-UAV to Monitor Active Landslide Scenarios, in: Engineering Geology for Society and Territory, edited by: Lollino, G., Manconi, A., Guzzetti, F., Culshaw, M., Bobrowsky P., and Luino, F., Springer International Publishing Switzerland, 5, 701-704, https://doi.org/10.1007/978-3-319-09048-1_136, 2015.

Van Den Eeckhaut, M., Poesen, J., Verstraeten, G., Vanacker, V., Nyssen, J., Moeyersons, J., van Beek, L. P. H., and Vandekerckhove, L.: Use of LIDAR-derived images for mapping old landslides under forest, Earth Surf. Proc. Land., 32, 754-769, https://doi.org/10.1002/esp.1417, 2007.

Nat. Hazards Earth Syst. Sci. Discuss., doi:10.5194/nhess-2017-111, 2017
Manuscript under review for journal Nat. Hazards Earth Syst. Sci.
Discussion started: 3 April 2017

Natural Hazards and Earth System Sciences
Discussions

Table 1. Characteristics of the images used to identify and map the Assignano landslide (Fig. 1). O: order in the sequence of images shown to the interpreter. Platform used to capture the image: W, WorldView-2 satellite; U, UAV. Resolution (ground resolution), in meter. Spectral (image spectral composite): TCC, True Colour Composite (Red, Green, Blue); FCC, False Colour Composite (Near infrared, Red, Green). Type (image type): M, monoscopic; S, stereoscopic; P, pseudo-stereoscopic. Map: Corresponding landslide map (Fig. 2).

O	Platform	Resolution	Spectral	Type	Map
1	W	1.85	TC	M	C
2	W	1.85	FCC	M	D
3	W	1.85	TC	S	E
4	W	1.85	FCC	S	F
5	U	0.03	TC	M	G
6	U	0.03	TC	P	H

Nat. Hazards Earth Syst. Sci. Discuss., doi:10.5194/nhess-2017-111, 2017
Manuscript under review for journal Nat. Hazards Earth Syst. Sci.
Discussion started: 3 April 2017

Natural Hazards and Earth System Sciences Discussions

Table 2. Comparison of the total landslide area (A_L), the landslide source and transportation area (A_{LS}), the landslide deposit (A_{LD}), the width and length of the entire landslide (W_L, L_L), of the source and transportation area (W_{LS}, L_{LS}), and of the deposit (W_{LD}, L_{LD}), for eight separate and independent cartographic representations of the Assignano landslide. EL, entire landslide; ST, landslide source and transport area; LD, landside deposit. See Table 3 for the characteristics of the single maps.

		Map A	Map B	Map C	Map D	Map E	Map F	Map G	Map H
Landslide area (m^2)									
EL	A_L	1.11×10^4	1.91×10^4	1.53×10^4	1.52×10^4	1.09×10^4	1.06×10^4	1.19×10^4	1.16×10^4
ST	A_{LS}	5.40×10^3	7.40×10^3	3.64×10^3	4.02×10^3	5.71×10^3	6.03×10^3	5.21×10^3	5.70×10^3
LD	A_{LD}	5.73×10^3	1.17×10^4	1.16×10^4	1.12×10^4	5.15×10^3	4.59×10^3	6.70×10^3	5.87×10^3
Landslide length (m) and width (m)									
EL	W_L	70.7	97.8	113.4	109.9	61.4	61.25	89.9	85.3
	L_L	362.0	387.5	404.7	391.2	354.6	359.5	343.3	349.1
ST	W_{LS}	51.5	59.6	43.6	49.2	51.92	54.3	49.5	50.5
	L_{LS}	227.9	229.7	205.9	208.0	239.0	239.2	234.7	237.3
LD	W_{LD}	61.0	98.69	111.5	109.0	56.0	57.6	89.9	81.9
	L_{LD}	152.7	172.1	206.2	203.5	129.8	134.7	139	121.8

Nat. Hazards Earth Syst. Sci. Discuss., doi:10.5194/nhess-2017-111, 2017
Manuscript under review for journal Nat. Hazards Earth Syst. Sci.
Discussion started: 3 April 2017

Natural Hazards and Earth System Sciences Discussions

Table 3. Comparison of the estimated cost, acquisition and pre-processing time, and storage requirement for an area of 4 km^2 (2 km × 2 km) and for an area of 100 km^2 (10 km × 10 km), for monoscopic and stereoscopic satellite images, and for an area of 15 km^2 for photographic images captured by an UAV.

	Satellite monoscopic		Satellite stereoscopic		UAV	
	4 km^2	100 km^2	4 km^2	100 km^2	4 km^2	15 km^2
Acquisition cost (€)	1.500	1.500	3.500	3.500	1.000	3.000
Pre-processing cost (€)	50	50	50	50	250-300	3.000
Acquisition time (day/person)	7-60	7-60	7-60	7-60	1	4
Pre-processing time (hr/person)	1	1	1	1	5-6	20-24
Storage (GB)	0.5	0.5	1	1	12	50
Resolution (m)	2	2	2	2	0.02	0.02
Morphologic signature	no	no	yes	yes	yes	yes
Photographic signature	yes	yes	yes	yes	yes	yes

Nat. Hazards Earth Syst. Sci. Discuss., doi:10.5194/nhess-2017-111, 2017
Manuscript under review for journal Nat. Hazards Earth Syst. Sci.
Discussion started: 3 April 2017

Natural Hazards and Earth System Sciences
Discussions

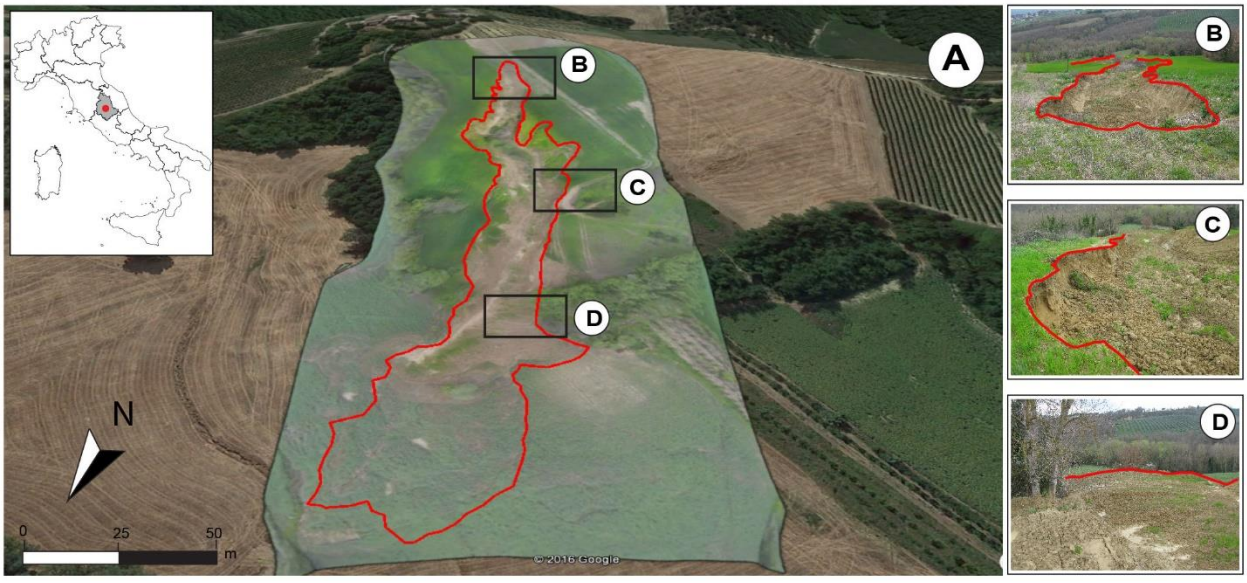

Figure 1. The Assignano landslide, located near Collazzone, Umbria, central Italy. (A) global view of the landslide. (B) detail of the landslide source area. (C) detail of the landslide transportation area. (D) detail of the landslide deposit.

Nat. Hazards Earth Syst. Sci. Discuss., doi:10.5194/nhess-2017-111, 2017
Manuscript under review for journal Nat. Hazards Earth Syst. Sci.
Discussion started: 3 April 2017

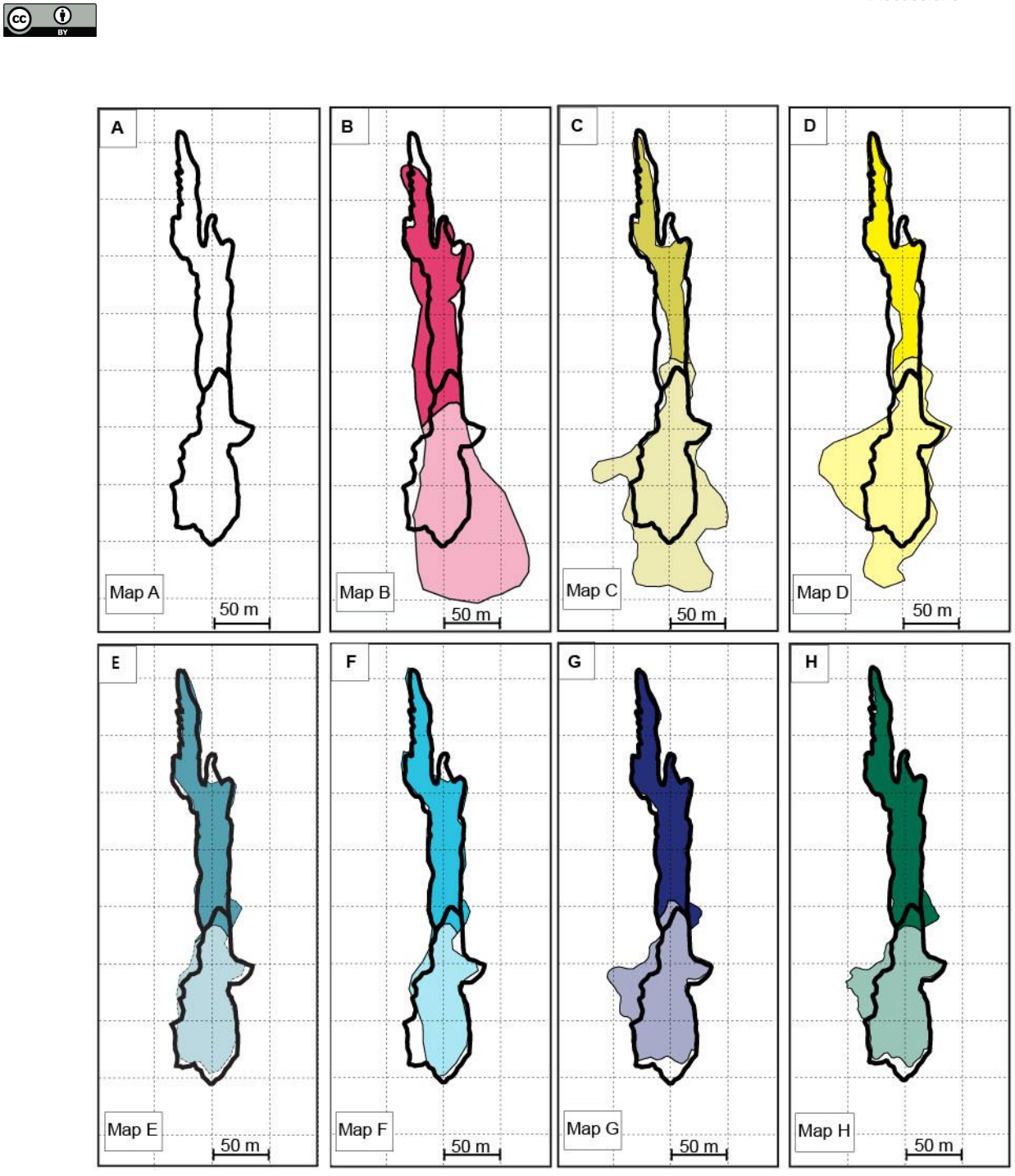

Figure 2. Eight independent cartographic representations of the Assignano landslide, "Map A" to "Map H". Map A obtained through a RTK DGPC survey is considered the "benchmark", and shown as a thick black line in the other maps. Map B obtained through reconnaissance field mapping. Map C to Map F obtained through the expert visual interpretation of the satellite images. Map G and Map H obtained through the expert visual interpretation of image taken by the UAV. See Table 1 for image characteristics. Dark colours show the landslide source and transportation area.

Nat. Hazards Earth Syst. Sci. Discuss., doi:10.5194/nhess-2017-111, 2017
Manuscript under review for journal Nat. Hazards Earth Syst. Sci.
Discussion started: 3 April 2017

Natural Hazards and Earth System Sciences
Discussions

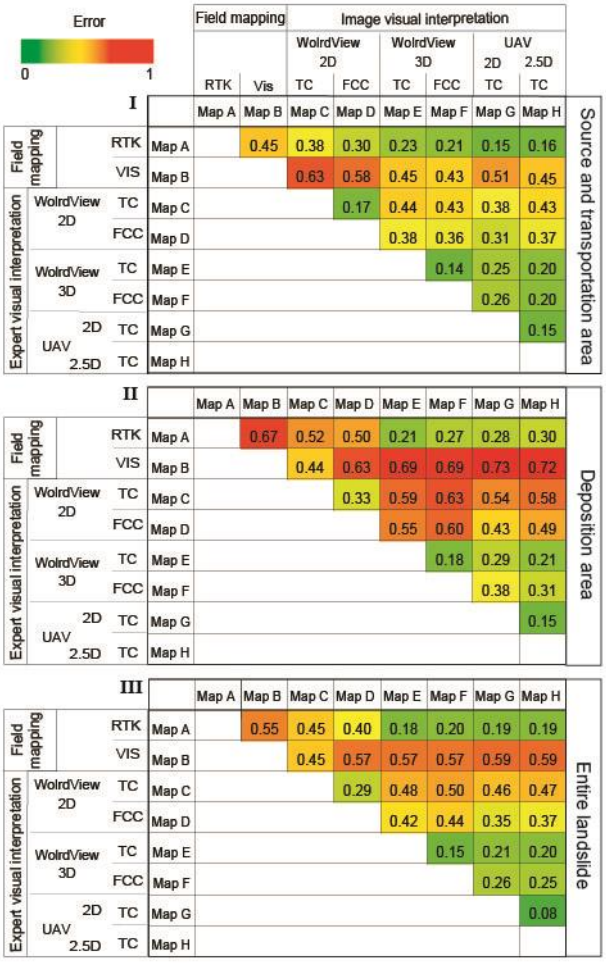

Figure 3. Error matrix obtained from a pairwise comparison of different landslide maps prepared for the Assignano landslide, Umbria, Central Italy. (I) Error matrix for the landslide source and transportation area. (II) Error matrix for the landslide deposit. (III) Error matrix for the entire landslide.

Nat. Hazards Earth Syst. Sci. Discuss., doi:10.5194/nhess-2017-111, 2017
Manuscript under review for journal Nat. Hazards Earth Syst. Sci.
Discussion started: 3 April 2017

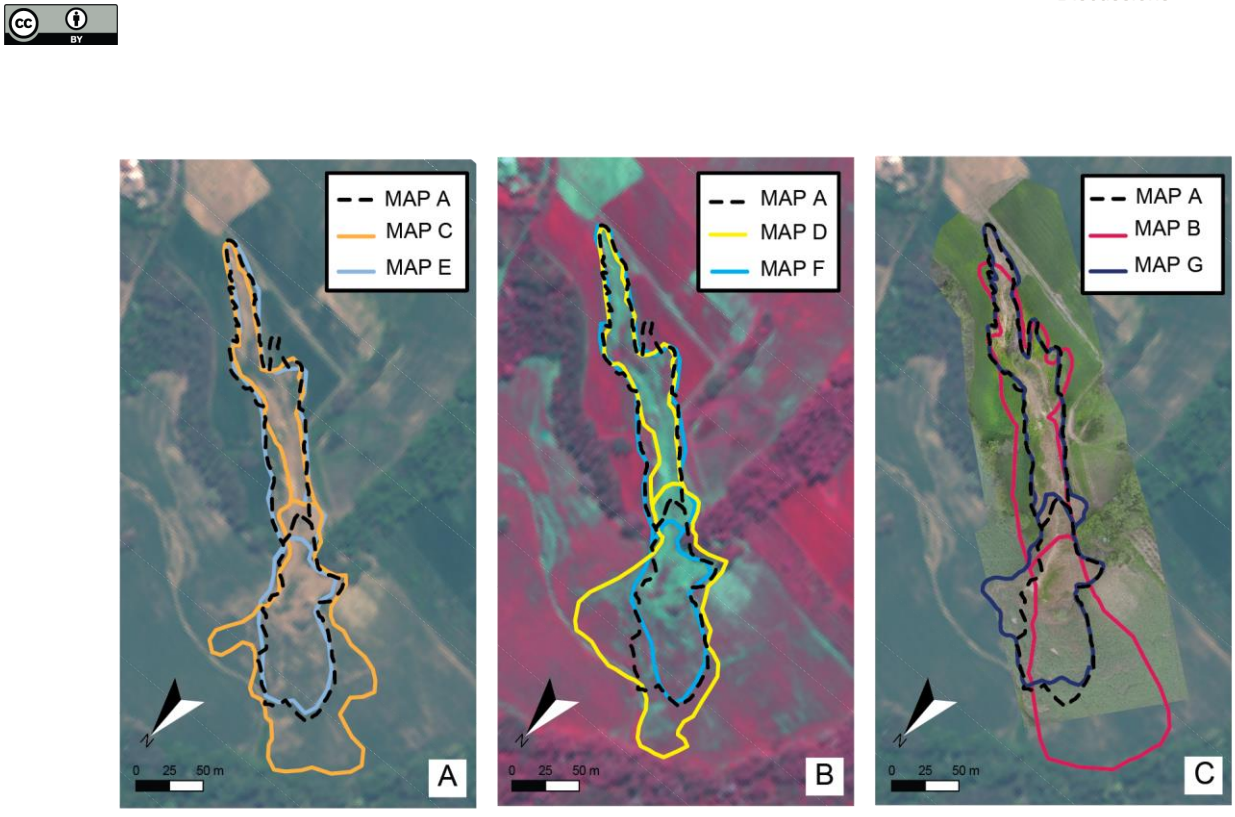

Figure 4. Comparison of landslide maps prepared for the Assignano landslide, Umbria, Central Italy. (A) Landslide map obtained from a monoscopic (Map C, dark yellow line) and a stereoscopic (Map E, light blue line), true-colour (TC) WordView-2 satellite image (base image), and a mapping of the landslide obtained by walking a GPS receiver along the landslide boundary (Map A, black line). (B) Landslide map obtained from a monoscopic (Map D, yellow line) and a stereoscopic (Map F, cyan line), false-colour-composite (FCC) WordView-2 satellite image, and a mapping obtained by walking a GPS receiver along the landslide boundary (Map A, black line). (C) Landslide map obtained from field survey (Map B, pink line) and from a monoscopic, TC, ultra-resolution image captured by an UAV (Map G, purple line), and the mapping obtained by walking a GPS receiver along the landslide boundary (Map A, black line).